How to cite: Angew. Chem. Int. Ed. 2024, e202319874
doi.org/10.1002/anie.202319874

Chiral Nanographenes

Enhancing Chiroptical Responses in Helical Nanographenes via Geometric Engineering of Double [7]Helicenes

Wenhui Niu[+],* *Yubin Fu*[+], *Qingsong Deng, Zhen-Lin Qiu, Fupin Liu, Alexey A. Popov, Hartmut Komber, Ji Ma,* and Xinliang Feng*

Abstract: Helical nanographenes with high quantum yields and strong chiroptical responses are pivotal for developing circularly polarized luminescence (CPL) materials. Here, we present the successful synthesis of novel π-extended double [7]helicenes (**ED7Hs**) where two helicene units are fused at the *meta*- or *para*-position of the middle benzene ring, respectively, as the structural isomers of the reported *ortho*-fused **ED7H**. The structural geometry of these **ED7Hs** is clearly characterized by single-crystal X-ray analysis. Notably, this class of **ED7Hs** exhibits bright luminescence with high quantum yields exceeding 40 %. Through geometric regulation of two embedded [7]helicene units from *ortho*-, *meta*- to *para*-position, these **ED7Hs** display exceptional amplification in chiroptical responses. This enhancement is evident in a remarkable approximate fivefold increase in the absorbance and luminescence dissymmetry factors (g_{abs} and g_{lum}), respectively, along with a boosted CPL brightness up to 176 $M^{-1}cm^{-1}$, surpassing the performance of most helicene-based chiral NGs. Furthermore, DFT calculations elucidate that the geometric adjustment of two [7]helicene units allows the precise alignment of electric and magnetic transition dipole moments, leading to the observed enhancement of their chiroptical responses. This study offers an effective strategy for magnifying the CPL performance in chiral NGs, promoting their expanded application as CPL emitters.

Introduction

Helical nanographenes (NGs) bearing [n]helicene motifs possess inherent chirality and intriguing chiroptical properties,[1] which make them suitable for various applications such as chiral-induced spin selectivity (CISS),[2] organic spintronics,[3] and particularly in the field of circularly polarized luminescence (CPL) materials.[4] To quantitatively evaluate the overall efficiency of helical NGs as CPL emitters, a new parameter known as CPL brightness (B_{CPL}) has been introduced recently.[5] B_{CPL} can be calculated using the formula $B_{CPL}=\varepsilon\times\Phi_f\times g_{lum}/2$, where ε *is* the molar extinction coefficient, Φ_f presents fluorescence quantum yield, and g_{lum} is the luminescence dissymmetry factor. To develop CPL materials with elevated B_{CPL} in helicene-based chiral NGs, the primary challenge revolves around achieving a delicate balance between ensuring high Φ_f and significant g_{lum} (Figure 1a), given their minor variations in extinction coefficients.[6] Until now, the g_{lum} in previously reported helical NGs have mostly remained at the level of 10^{-3},[7] and their Φ_f values have usually fallen below 30 %,[8] leading to modest B_{CPL} values, usually falling below 90 $M^{-1}cm^{-1}$ (Figure 1a).[9] In recent years, substantial efforts have been dedicated to improving the values of Φ_f and g_{lum} in helical NGs, aiming to achieve high B_{CPL} values. For example, Wang et al. reported a strategy to improve Φ_f by helical π-extension of highly emissive perylene while maintaining its frontier molecular orbital distribution pattern. Consequently, the resultant double [6]helicene exhibited an exceptionally high Φ_f up to 93 %. However, the achieved B_{CPL}

[*] Dr. W. Niu,[+] Dr. Y. Fu,[+] Dr. J. Ma, Prof. Dr. X. Feng
Max Planck Institute of Microstructure Physics, Weinberg 2, Halle 06120 Germany
E-mail: wenhui.niu@mpi-halle.mpg.de
ji.ma@mpi-halle.mpg.de

Dr. W. Niu,[+] Dr. Y. Fu,[+] Dr. Z.-L. Qiu, Dr. J. Ma, Prof. Dr. X. Feng
Center for Advancing Electronics Dresden (cfaed) & Faculty of Chemistry and Food Chemistry, Technische Universität Dresden Mommsenstrasse 4, 01062 Dresden, Germany

Q. Deng
State Key Laboratory for Physical Chemistry of Solid Surfaces and Department of Chemistry, College of Chemistry and Chemical Engineering, Xiamen University, Xiamen 361005, P. R. China

Dr. F. Liu, Dr. A. A. Popov
Leibniz Institute for Solid State and Materials Research, 01069 Dresden, Germany

Dr. H. Komber
Leibniz-Institut für Polymerforschung Dresden e. V., Hohe Straße 6, 01069 Dresden, Germany

Dr. J. Ma
College of Materials Science and Opto-Electronic Technology & Center of Materials Science and Optoelectronics Engineering, University of Chinese Academy of Science, 100049 Beijing, P. R. China

[+] These authors contributed equally to this work.

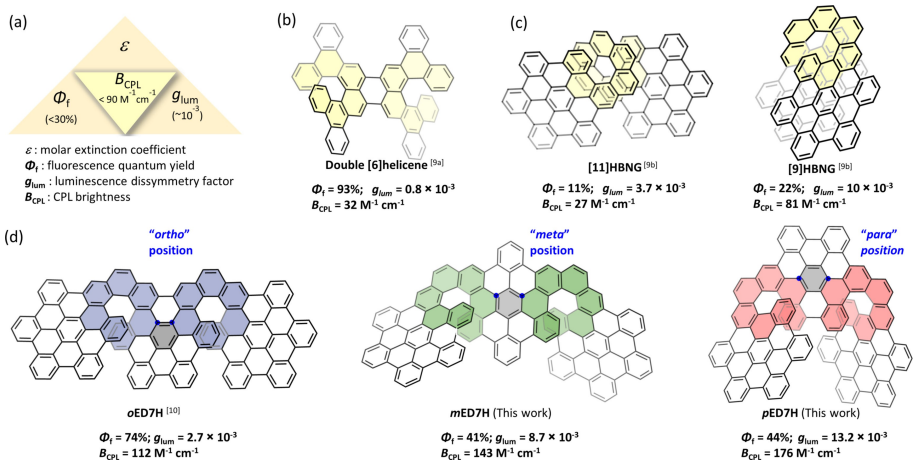

Figure 1. (a) The key factors in defining the CPL brightness. Reported examples to synthesize π-extended helicenes with increasing Φ_f (b) or upgrading g_{lum} (c). (d) π-extended double [7]helicenes (**ED7Hs**) presented in this work with high Φ_f (>40%), amplified g_{lum}, as well as boosted B_{CPL} up to 176 $M^{-1}cm^{-1}$ via geometric engineering of helicene units from *ortho*-, *meta*-, to *para*-position. Their *PP* enantiomers are depicted as representatives and all ^{t}Bu groups are omitted for clarity.

value was relatively modest at 32 $M^{-1}cm^{-1}$ due to its low g_{lum} value of 0.8×10^{-3} (Figure 1b).[9a] Recently, Martín et al. reported the remarkably amplified g_{lum} in helical bilayer NGs (HBNG) by tuning the overlapping degree of [n]helicene-based bilayer units, affording the high B_{CPL} of 81 $M^{-1}cm^{-1}$ for [9]HBNG, calculated based on the Φ_f of 22% and enhanced g_{lum} of 10×10^{-3} (Figure 1c).[9b] Despite the above progress, the strategies for maintaining high Φ_f (>30%) while simultaneously increasing the g_{lum} remain elusive, impeding the advancement of CPL emitters based on helical NGs.

Herein, we demonstrate the successful synthesis of a series of π-extended helical NGs bearing double [7]helicenes (**ED7Hs**) where the two [7]helicene units are fused at *meta*-(***m*ED7H**) or *para*-position (***p*ED7H**) of the middle benzene ring, respectively, differing from the previously reported ***o*ED7H** where helicenes are fused at the *ortho*-position (Figure 1d).[10] Their distinct geometry has been thoroughly characterized by single-crystal analysis, revealing the increased interlayer distances of ***m*ED7H** and ***p*ED7H**, compared to that of ***o*ED7H**. Interestingly, ***m*ED7H** and ***p*ED7H** display bright luminescence with high Φ_f above 40%, larger than most of the reported π-extended helical NGs.[7a,8b, 9b, 11] The embedded double [7]helicenes provide inherent chirality and good conformational stability with the high isomerization barrier of 67 kcal mol^{-1}, allowing their chiral resolution and investigation of chiroptical properties. Notably, ***m*ED7H** and ***p*ED7H** demonstrate significantly amplified g_{abs} up to 10×10^{-3} at 546 nm and 18×10^{-3} at 540 nm, respectively, with a remarkable 2.6-fold and 4.6-fold increase compared to that of ***o*ED7H** (3.9×10^{-3} at 560 nm). DFT calculations revealed the well-alignment of magnetic transition dipole moment (μ_m) and electric transition dipole moment (μ_e), profiting from the geometry regulation of two [7]helicene units from *ortho*, *meta* to *para* position. Moreover, in comparison with the g_{lum} of ***o*ED7H** (2.7×10^{-3}), the exceptional 3.2-fold and 4.8-fold enhancement of g_{lum} are observed for ***m*ED7H** (8.7×10^{-3}) and ***p*ED7H** (13.2×10^{-3}), respectively. Thanks to the high Φ_f and boosted g_{lum}, this class of **ED7Hs** presents progressively increasing CPL brightness up to 176 $M^{-1}cm^{-1}$, superior to the majority of reported helical NGs, positioning them as promising candidates for CPL emitters. This work offers a novel design strategy to achieve double helicenes embedded chiral NGs with high chiroptical responses, which will stimulate the exploration of their potential applications in chiroptic devices.

Results and Discussion

The synthetic route to the structural isomers, ***m*ED7H** and ***p*ED7H**, is depicted in Scheme 1a. First, 2-(6-((4-(*tert*-butyl)phenyl)ethynyl)phenanthren-3-yl)-4,4,5,5-tetramethyl-1,3,2-dioxaborolane (**1**) was prepared in 72% yield by borylation reaction from 3-bromo-6-((4-(*tert*-butyl)phenyl)ethynyl)phenanthrene. Then, the two-fold Suzuki coupling of 4,4″-di-*tert*-butyl-4′,5′-bis(4-(*tert*-butyl)phenyl)-3′,6′-diiodo-1,1′:2′,1″-terphenyl (**2**) and compound **1** gave 6,6′-(4,4″-di- tert-butyl-4′,5′-bis(4-(tert-butyl)phenyl)-[1,1′:2′,1″-terphenyl]-3′,6′-diyl)bis(3-((4-(*tert*-butyl)phenyl)ethynyl)phenanthrene) (**3**) in 78% yield. Subsequently, Diels–Alder reaction with 2,3,4,5-tetrakis(4-(*tert*-butyl)phenyl)cyclopenta-2,4-dien-1-one (**4**) furnished the corresponding precursor 6,6′-(4,4″-di-*tert*-butyl-4′,5′-bis(4-(*tert*- butyl)phenyl)-[1,1′:2′,1″-terphenyl]-3′,6′-diyl)bis(3-(4,4″-di-*tert*-butyl-4′,5′,6′-tris(4-(*tert*-butyl)phenyl)-[1,1′:2′,1″-terphenyl]-3′-yl)phenanthrene) (**5**) in 91% yield. Finally, the intramolecular Scholl reaction of **5** using 2,3-dichloro-5,6-dicyano-1,4-benzoquinone (DDQ) and trifluoromethanesulfonic acid (TfOH) gave the desired π-extended double [7]helicenes that were fused at the *para*-position, affording the *racemic* conformer (***p*ED7H**-*PP* and *MM*) in 45% isolated yield. Due to the high regioselectivity, no *S*-shaped

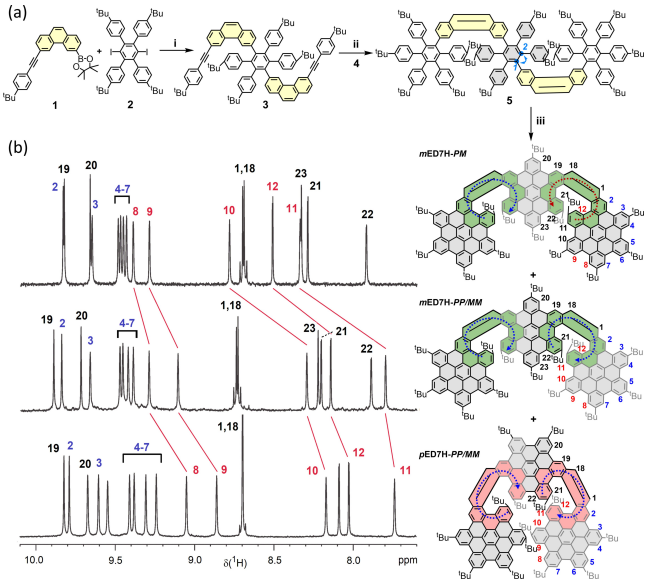

Scheme 1. (a) Synthetic route to π-extended double [7]helicenes (***m*ED7H** and ***p*ED7H**). The blue arrows present the chirality of each [7]helicene. Clockwise: *P*; Counterclockwise: *M*. (i) $Pd(PPh_3)_4$, K_2CO_3, dioxane, H_2O, 95 °C, 24 h, 78 %; (ii) Tetrakis(4-(*tert*-butyl)phenyl)cyclopenta-2,4-dien-1-one (**4**), Ph_2O, 270 °C, 24 h, 91 %; (iii) DDQ, DCM, TfOH, 0 °C, 40 min, 45 % for ***p*ED7H**-*PP*, 6 % for ***m*ED7H**-*PP* and 2 % for ***m*ED7H**-*PM*. (b) ^{1}H NMR spectra (region) of ***m*ED7H**-*PM*, ***m*ED7H**-*PP* and ***p*ED7H**-*PP* (CD_2Cl_2). The lines point to the shielding effects for the inner protons of the terminal HBC units (red, 8–12) going from *PM* to *PP* isomer of ***m*ED7H** and for ***p*ED7H**-*PP*. The chemical shifts of the outer protons (blue, 2–7) remain almost unchanged.

products, where the two phenanthrene units are fused at the opposite side of the middle HBC molecules, were observed during the Scholl reaction. Interestingly, due to the 1,2-aryl exchange in **5** during the cyclodehydrogenation process (highlighted in blue in Scheme 1a), unexpected products were also achieved wherein the double [7]helicene fused at the *meta*-position, affording both the *racemic* conformer (***m*ED7H**-*PP* and *MM*) and *meso* conformer (***m*ED7H**-*PM*) in isolated yields of 6 % and 2 %, respectively.

The structural identities of the obtained **ED7Hs** were first confirmed via high-resolution matrix-assisted laser desorption/ionization time-of-flight (MALDI-TOF) mass spectrometry (Figure S1). The ***p*ED7H** and ***m*ED7H** possess identical chemical formulas and mass signals, in which the calculated isotopic distribution patterns are consistent with the experimental results. The ^{1}H NMR spectra align well with the anticipated structures of ***p*ED7H** and ***m*ED7H**, and all signals have been successfully assigned with the help of 2D NMR techniques (Figures S2–S18; Table S1, S2). Furthermore, the different helicity of the *PM* and *PP* isomer of ***m*ED7H** leads to characteristic chemical shifts for the aromatic protons of the outer hexabenzocoronene (HBC) units, which are directed towards the middle HBC unit (H_8-H_{12}). A significant shielding effect is observed for these protons in the screw-type *PP* isomer compared to the *PM* isomer of ***m*ED7H** (Scheme 1b, indicated by red lines). This shielding is also evident for the *PP* isomer of ***p*ED7H** and is observed for the *PP*/*PM* isomer pair of ***o*ED7H**.[10] The geometry of these screw-type *PP* isomers results in an enhanced shielding effect of the extended HBC π-ring systems on these protons compared to the *PM* isomers (Table S3, S4). This feature could be helpful for a quick identification of different helicities of helical NGs.

The distinct alignment of two [7]helicene units within ***m*ED7H** and ***p*ED7H** was unambiguously confirmed by single-crystal analysis, wherein the [7]helicene units are highlighted accordingly (Figure 2a–c). [12] The single crystals of ***m*ED7H** and ***p*ED7H** were grown by slow evaporation of methanol into chlorobenzene solution of their *racemic* mixture, respectively. The interlayer distances of adjacent HBC layers can be evaluated by the centroid-centroid distances of the terminal benzene rings of [7]helicene units. Accordingly, the interlayer distances of ***m*ED7H** (4.21 Å, 3.81 Å) and ***p*ED7H** (3.96 Å, 4.04 Å) have been found significantly enlarged compared to that of ***o*ED7H** (3.26 Å, 3.57 Å), suggesting reduced interlayer π–π interaction. The different interlayer interactions of ***o***, ***m***, and ***p*ED7H** were also examined by DFT calculations based on an independent gradient model based on the Hirshfeld partition (IGMH) method (Figure S21).[13] The calculation results visualize the attractive interlayer interactions for ***o***, ***m***, ***p*ED7H**, showing obvious van der Waals interactions (green surface) between three layers. The index δ_g can quantify the total interaction between each layer, revealing the decreasing δ_g of 5.42 for ***o*ED7H**, 4.57 for ***m*ED7H**, and 3.94 for ***p*ED7H**, respectively, as a result of the diminishing interlayer interactions attributed to the regulation of two helicene units from *ortho*-, *meta*- to *para*-position. For crystal packing of ***m*ED7H** and ***p*ED7H**, the homochiral isomers are arranged

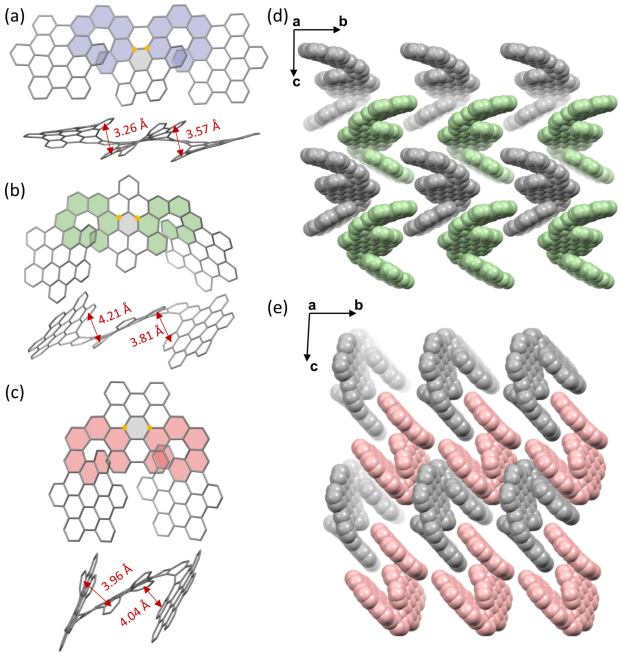

Figure 2. Single-crystal structures of ***o*ED7H** (a), ***m*ED7H** (b), and ***p*ED7H** (c). Crystal packing of ***m*ED7H** (d), and ***p*ED7H** (e). Solvent molecules and ^{t}Bu groups are omitted for clarity.

along the *a*-axis, resulting in *P* and *M* isomers that appear alternately in the unit cell (Figure 2d–e).

To evaluate the optical properties of the *racemic* isomers of ***o***, ***m***, and ***p*ED7H**, their UV/Vis and emission spectra were recorded in anhydrous dichloromethane (DCM) with the concentration of 1×10^{-5} M and ~1×10^{-6} M, respectively (Figure 3a). Compared to ***o*ED7H**, ***m*ED7H** and ***p*ED7H** exhibited the slight-blue-shift absorption with the maximum absorption peaks (λ_{max}) of 543 and 533 nm (Figure 3a, solid lines). According to the absorption onsets, the energy gaps were calculated to be 2.19 eV for ***m*ED7H** and 2.21 eV for ***p*ED7H**, respectively, slightly larger than that of ***o*ED7H** (2.12 eV). In addition, the emission spectra of ***m*ED7H** and ***p*ED7H** in anhydrous DCM (Figure 3a, dashed lines) featured the blue-shift fluorescence spectra at 564 and 562 nm, respectively, in comparison with that of ***o*ED7H** (577 nm). Notably, ***m*ED7H** and ***p*ED7H** presented strong fluorescence with quantum yields of 41 % and 44 %, surpassing those reported π-extended NGs with larger conjugated structures[7a,8b, 9b, 11] that can be attributed to the significant overlap of electron and hole distributions (Figure S22). In addition, the transient photoluminescence spectra were also recorded for ***o*ED7H**, ***m*ED7H**, and ***p*ED7H**, revealing fluorescence lifetimes of 5.46, 8.48, and 8.17 ns, respectively (Figure S29 and Table S10). Moreover, cyclic voltammetry (CV) was used to study the electrochemical properties of ***o***, ***m***, and ***p*ED7H** in anhydrous DCM (Figure 3b). For all three **ED7Hs**, three reversible oxidation waves were observed, with half-wave potential $E_{ox}^{1/2}$ of 0.36, 0.55, and 0.80 V (*vs* Fc^+/Fc) for ***o*ED7H**, 0.37, 0.53, and 0.73 V (*vs* Fc^+/Fc) for ***m*ED7H**, and 0.36, 0.50, and 0.72 V (*vs* Fc^+/Fc) for ***p*ED7H**. According to the onset potentials of the first oxidation waves, the HOMO levels are estimated to be consistent at −5.11 eV for these **ED7Hs**. To gain deeper insight into the electronic structures of this series of **ED7Hs**, DFT calculations at B3LYP-D3(BJ)/6-31G(d) level were performed (Figure 3c). Compared to ***o*ED7H**, ***m*ED7H** and ***p*ED7H** present higher LUMO energy levels (−2.03 eV for ***o*ED7H**, −1.92 eV for ***m*ED7H**, and −1.92 eV for ***p*ED7H**); meanwhile, the HOMO energy levels keep roughly at the same values (−4.71 eV for ***o*ED7H**, −4.70 eV for ***m*ED7H**, and 4.70 eV for ***p*ED7H**), leading to the slightly enlarged energy gaps, in good agreement with the experimental results. In addition, TD-DFT calculations give more insight into the fluorescence process. Calculation results revealed the emission peaks of ***o***, ***m***, and ***p*ED7H** to be 587 nm, 585 nm, and 585 nm, which can be assigned to the LUMO→HOMO transition (Figure 3c).

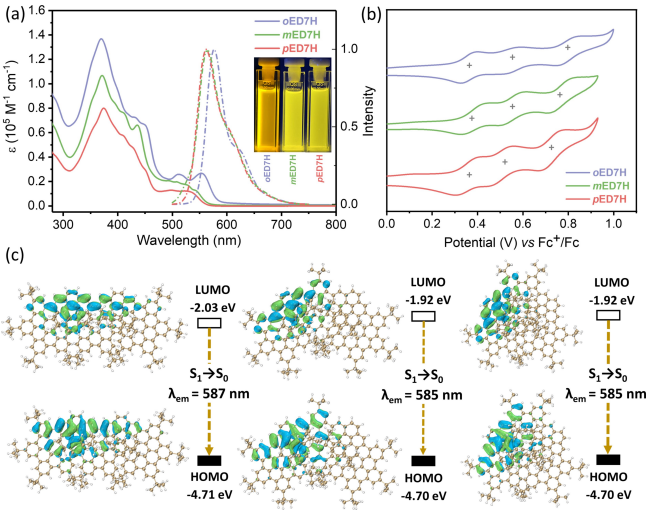

Figure 3. (a) UV–Vis absorption spectra (solid lines) and fluorescence spectra (dashed lines) of ***o***, ***m***, and ***p*ED7H**-*PP*/*MM* in anhydrous DCM. The inset shows photographs of the *racemic* isomers of ***o*ED7H**, ***m*ED7H** and ***p*ED7H** in DCM solution under UV light illumination. (b) CV of ***o***, ***m***, and ***p*ED7H** in DCM containing 0.1 M *n*-Bu_4NPF_6 at a scan rate of 0.1 $V\,s^{-1}$. (c) Molecular orbitals at the excited state and the emission wavelength of ***o***, ***m***, and ***p*ED7H** calculated at the B3LYP-D3(BJ)/6-31G(d) level.

To assess the conformational stability of the resultant **ED7Hs**, their isomerization process was calculated by DFT simulations at the basic set B3LYP-D3(BJ)/6-31G(d) (Figures S30–31). For both ***m*ED7H** and ***p*ED7H**, the *racemic* products (*PP*/*MM*) are thermodynamically more stable than *meso* product (*PM*) by 10.2 and 5.0 kcal mol^{-1}, respectively. The isomerization barrier from ***m*ED7H**-*PP* to ***m*ED7H**-*PM* was estimated to be 67.2 kcal mol^{-1}. Similarly, the isomerization barrier from the *racemic* product to *meso* product of ***p*ED7H** was calculated to be 72.7 kcal mol^{-1}. The calculated energy barriers reported here are much higher than that of the double [7]helicene based systems reported so far,[14] demonstrating the rigid backbone and excellent chirality stability of **ED7Hs**.[15] Moreover, we examined the thermal stability of ***m*ED7H**-*PP* in 1,2-dichlorobenzene under 180 °C for 24 h, the comparison of HPLC curves presents the remained clean peak from ***m*ED7H**-*PP*, indicating the high thermal stability for this class of helical NGs (Figure S32). This characteristic allows us to achieve the racemic resolution of ***m*ED7H** and ***p*ED7H** by chiral high-performance liquid chromatography (HPLC). The successful chiral resolution yielded the optically pure ***m*ED7H**-*PP*/*MM* and ***p*ED7H**-*PP*/*MM*, respectively (Figures S33–34), with the chirality of each enantiomer assigned with the assistance of theoretical studies (Figure 4a–c, grey lines). Subsequently, the chiroptical properties of the pure enantiomers of ***mED7H***-*PP*/*MM* and ***p*ED7H**-*PP*/*MM* were investigated by CD and CPL spectroscopies, compared to those of reported ***o*ED7H**-*PP*/*MM*. As shown in Figure 4a–c, enantiomerically pure ***o***, ***m***, and ***p*ED7H** in DCM (1×10^{-5} M) exhibit Cotton effects with mirror-image CD spectra in the range of 280–600 nm. According to the equation $g_{abs}=\Delta\varepsilon/\varepsilon$, the relationship between g_{abs} and wavelength is described in Figure 4d. Notably, compared to ***o*ED7H** featuring maximum absorption dissymmetry factor (g_{abs}) of 3.9×10^{-3} at 560 nm, the g_{abs} values were found to be amplified to 10×10^{-3} at 546 nm for ***m*ED7H**, and further significantly boosted to 18×10^{-3} at 540 nm for ***p*ED7H** with an extraordinary 4.6-fold magnification in total. Subsequently, the CPL spectra of optically pure ***o***, ***m***, and ***p*ED7H**-*PP*/*MM* were measured in DCM (~1×10^{-6} M) and three pairs of enantiomers showed mirror-like images in the range of 540–650 nm with the full-width at half maximum (FWHM) of 38 nm, 46 nm and 45 nm,

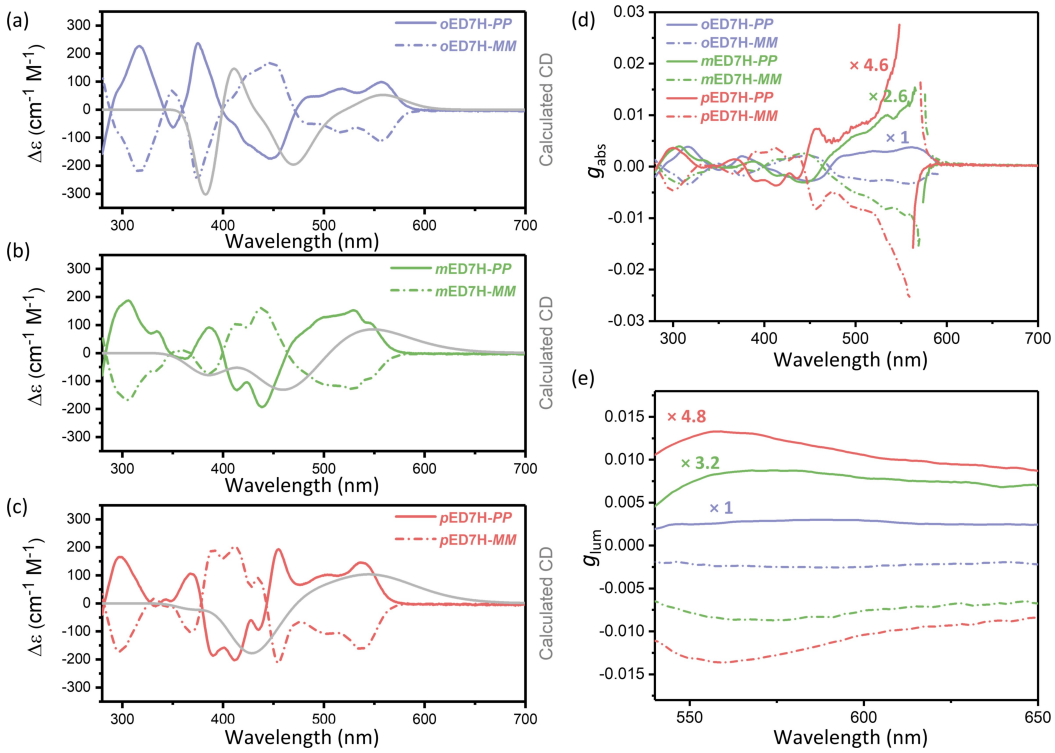

Figure 4. (a–c) Experimental CD spectra of the pure enantiomers of ***o***, ***m***, and ***p*ED7H**-*PP/MM* in anhydrous DCM in comparison with the calculated CD spectra of *PP* enantiomers. (d, e) g_{abs} and g_{lum} of ***o***, ***m***, and ***p*ED7H**-*PP/MM*.

respectively (Figure S35). Remarkably, similar to the trend of g_{abs}, the g_{lum} exhibited a conspicuous rise, reaching up to $+8.7\times10^{-3}/-8.7\times10^{-3}$ at 565 nm for ***m*ED7H**-*PP/MM* and $+13.2\times10^{-3}/-13.5\times10^{-3}$ at 556 nm for ***p*ED7H**-*PP/MM*, respectively (Figure 4e), with the exceptional 3.2-fold and 4.8-fold magnification compared to the g_{lum} value of ***o*ED7H**-*PP/MM* ($+2.7\times10^{-3}/-2.5\times10^{-3}$ at 580 nm). The indisputable enhancement in both g_{abs} and g_{lum} proves that the geometry regulation of a multi-helicene system is an efficient strategy for enhancing both absorption and emissive chiroptical responses.

To explain the significant enhancement of dissymmetry factors and establish the relationship between the geometry of double [7]helicenes and their chiroptical properties, TD-DFT calculations were performed at B3LYP/6-31G(d) level (Figure 5a–g). The results reveal that the maximum g_{abs} of ***o***, ***m***, and ***p*ED7H**-*PP/MM* at 560 nm, 546 nm and 540 nm can be assigned to the $S_0\rightarrow S_1$ transition, where the related electric transition dipole moments (μ_e), magnetic transition dipole moments (μ_m) as well as the angle between them (θ) are shown in Figure 5. Based on the formula $g=4\cos\theta\times|\mu_m|/|\mu_e|$, both the value of $\cos\theta$ and the ratio of $|\mu_m|/|\mu_e|$ play important roles in determining the g value. The calculation results further show that, through the geometric engineering of two [7]helicene units from *ortho*-, *meta*- to *para*-positions, the θ and μ_e gradually decrease, while μ_m remains at a constant level. This leads to a simultaneous increase in $\cos\theta$ and $|\mu_m|/|\mu_e|$, consequently resulting in a significant boost of g_{abs}^{cal} of 1.3×10^{-3} for ***o*ED7H**, 7.2×10^{-3} for ***m*ED7H** and 22×10^{-3} for ***p*ED7H**, well supporting the experiment trend (Figure 5g). Furthermore, TD-DFT calculations on their excited state ($S_1\rightarrow S_0$ transition) were performed at the B3LYP/6-31G(d) level to deduce the origin of the increased g_{lum} values (Figure 5d–f). Similar to the CD calculations, a comparison with ***o*ED7H** reveals a simultaneously increase in $\cos\theta$ and $|\mu_m|/|\mu_e|$ for ***m*ED7H** and ***p*ED7H**, affording the increased g_{lum}^{cal} values of 1.8×10^{-3} for ***o*ED7H**, 4.0×10^{-3} for ***m*ED7H** and 5.0×10^{-3} for ***p*ED7H**. Thanks to the high Φ_f and progressively increased g_{lum}, the B_{CPL} values of ***m*ED7H** and ***p*ED7H** are estimated to be 143 and 176 $M^{-1}cm^{-1}$, respectively. These values are significantly elevated compared to that of ***o*ED7H** and surpass the majority of reported helicene-based NGs (Figure 5h, Table S11),[9–11] demonstrating their promising potential for CPL applications.

Conclusions

In summary, we have reported two novel π-extended double [7]helicenes, wherein the two helicene units were fused at *meta*- (***m*ED7H**) or *para*-position (***p*ED7H**) of the central benzene ring in the HBC unit. The structural geometries of ***m*ED7H** and ***p*ED7H** were unambiguously confirmed by single-crystal X-ray analysis, revealing the increased interlayer distance and reduced interlayer π–π interaction. The resultant **ED7Hs** exhibited high Φ_f over 40 %, profiting from the intense overlap of electron and hole distributions. The embedded two [7]helicene units provided a rigid backbone and high conformational stability, enabling the chiral

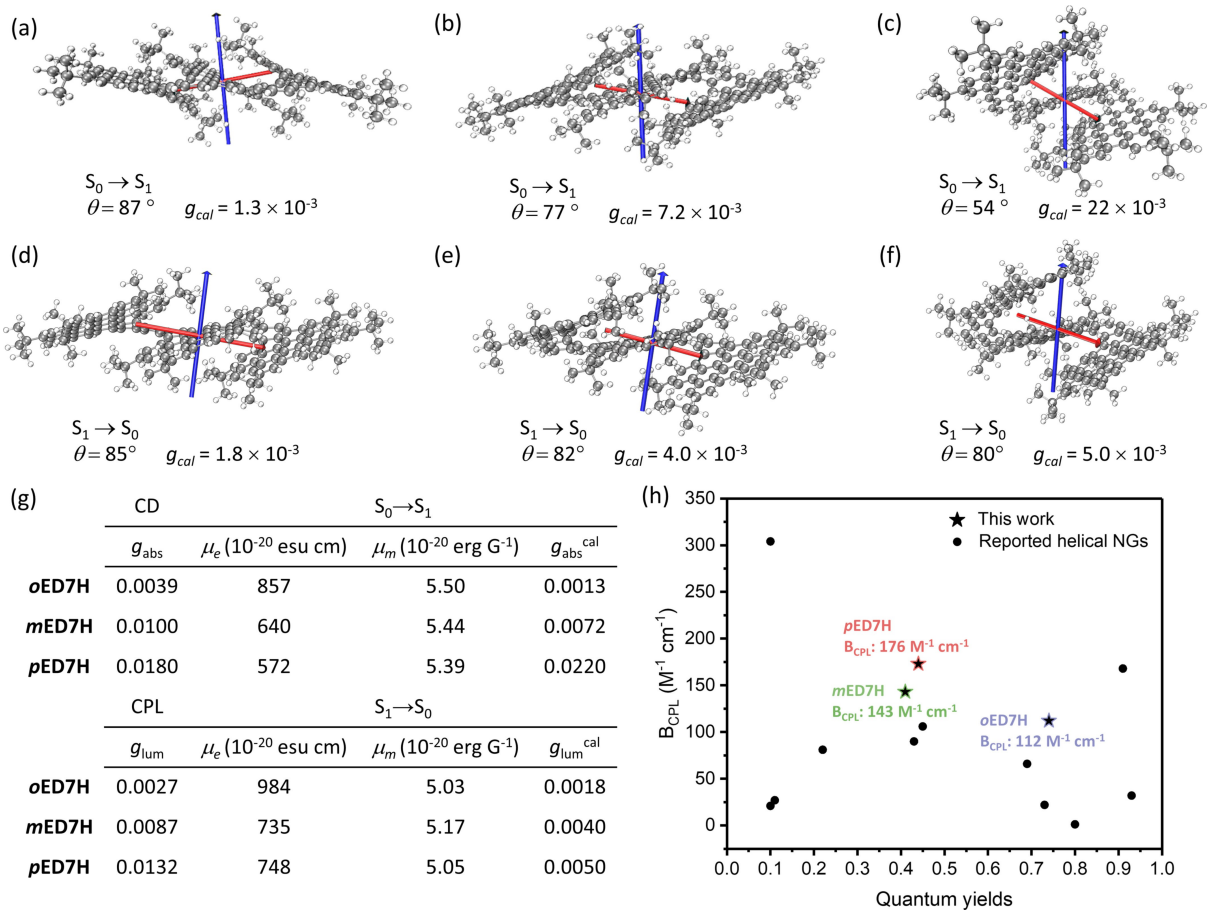

(g)

	CD		$S_0 \rightarrow S_1$	
	g_{abs}	μ_e (10^{-20} esu cm)	μ_m (10^{-20} erg G^{-1})	g_{abs}^{cal}
***o*ED7H**	0.0039	857	5.50	0.0013
***m*ED7H**	0.0100	640	5.44	0.0072
***p*ED7H**	0.0180	572	5.39	0.0220
	CPL		$S_1 \rightarrow S_0$	
	g_{lum}	μ_e (10^{-20} esu cm)	μ_m (10^{-20} erg G^{-1})	g_{lum}^{cal}
***o*ED7H**	0.0027	984	5.03	0.0018
***m*ED7H**	0.0087	735	5.17	0.0040
***p*ED7H**	0.0132	748	5.05	0.0050

Figure 5. (a–c) Transition dipole moments of ***o***, ***m***, and ***p*ED7H**-*PP/MM* for the $S_0 \rightarrow S_1$ transition, respectively. (d–f) Transition dipole moments of ***o***, ***m***, and ***p*ED7H**-*PP/MM* for the $S_1 \rightarrow S_0$ transition, respectively. The electric transition dipole moments (μ_e) and the magnetic transition dipole moments (μ_m) are shown in red and blue, respectively. The lengths of both electric and magnetic transition dipole moments are enlarged by 3 times. (g) Summary of chiroptical properties of ***o***, ***m***, and ***p*ED7H**-*PP/MM*. (h) Summary of the B_{CPL} values and quantum yields of the reported helical NGs and ***o***, ***m***, and ***p*ED7H**-*PP/MM* from this work.

separation of their enantiomers for CD and CPL spectroscopies. Notably, this series of **ED7Hs** displayed clear geometry-dependent chiroptical properties, disclosing significantly boosted g_{abs} and g_{lum} of ***m*ED7H** and ***p*ED7H**, compared to the values of ***o*ED7H**, which are further supported by DFT calculations. The high Φ_f and amplified g_{lum} contribute to the excellent B_{CPL} of this class of **ED7Hs**, reaching up to 176 $M^{-1}cm^{-1}$, superior to the most of reported helical NGs. This work introduces an effective strategy to boost the g values in helical NGs, facilitating the future design of multi-helicene-based NGs with outstanding CPL performance and stimulating their applications in chiral optoelectronics.

Acknowledgements

This research was financially supported by the EU Graphene Flagship (Graphene Core 3, 881603), ERC Consolidator Grant (T2DCP, 819698), H2020-MSCA-ITN (ULTIMATE, No. 813036), the Center for Advancing Electronics Dresden (cfaed), H2020-EU.1.2.2.—FET Proactive Grant (LIGHT-CAP, 101017821) and the DFG-SNSF Joint Switzerland-German Research Project (EnhanTopo, No. 429265950). The authors acknowledge the use of computational facilities at the Center for information services and high performance computing (ZIH) at TU Dresden. Diffraction data have been collected on BL14.2 at the BESSY II electron storage ring operated by the Helmholtz-Zentrum Berlin, and we appreciate the help of Manfred Weiss and his team during the experiments at BESSY II. The authors are grateful for the assistance of Mr. Karl-Ludwig Schumann from the B CUBE Center for Molecular Bioengineering in TU Dresden for the CD measurements and Dr. Li Wan from Max Planck Institute of Microstructure Physics for the CPL measurements. Open Access funding enabled and organized by Projekt DEAL.

Conflict of Interest

The authors declare no conflict of interest.

Data Availability Statement

The data that support the findings of this study are available from the corresponding author upon reasonable request.

Keywords: Helical Nanographenes · Chirality · Chiroptical Responses Amplification · Geometric Engineering · CPL Brightness

[1] a) Y. Zhu, J. Wang, *Acc. Chem. Res.* **2023**, *56*, 363–373; b) J. M. Fernández-García, P. J. Evans, S. Filippone, M. Á. Herranz, N. Martín, *Acc. Chem. Res.* **2019**, *52*, 1565–1574; c) Y. Zhang, S. H. Pun, Q. Miao, *Chem. Rev.* **2022**, *122*, 14554–14593; d) N. Ogawa, Y. Yamaoka, H. Takikawa, K.-i. Yamada, K. Takasu, *J. Am. Chem. Soc.* **2020**, *142*, 13322–13327; e) J. Ma, Y. Fu, E. Dmitrieva, F. Liu, H. Komber, F. Hennersdorf, A. A. Popov, J. J. Weigand, J. Liu, X. Feng, *Angew. Chem. Int. Ed.* **2020**, *59*, 5637–5642; f) L. Yang, Y.-Y. Ju, M. A. Medel, Y. Fu, H. Komber, E. Dmitrieva, J.-J. Zhang, S. Obermann, A. G. Campaña, J. Ma, X. Feng, *Angew. Chem. Int. Ed.* **2023**, *62*, e202216193; g) G. R. Kiel, H. M. Bergman, A. E. Samkian, N. J. Schuster, R. C. Handford, A. J. Rothenberger, R. Gomez-Bombarelli, C. Nuckolls, T. D. Tilley, *J. Am. Chem. Soc.* **2022**, *144*, 23421–23427.

[2] a) M. R. Safari, F. Matthes, C. M. Schneider, K.-H. Ernst, D. E. Bürgler, *arXiv preprint* **2023**, DOI: 10.48550/arXiv.2309.07588; b) V. Kiran, S. P. Mathew, S. R. Cohen, I. Hernández Delgado, J. Lacour, R. Naaman, *Adv. Mater.* **2016**, *28*, 1957–1962.

[3] R. Rodríguez, C. Naranjo, A. Kumar, P. Matozzo, T. K. Das, Q. Zhu, N. Vanthuyne, R. Gómez, R. Naaman, L. Sánchez, J. Crassous, *J. Am. Chem. Soc.* **2022**, *144*, 7709–7719.

[4] a) C. M. Cruz, S. Castro-Fernández, E. Maçôas, J. M. Cuerva, A. G. Campaña, *Angew. Chem. Int. Ed.* **2018**, *57*, 14782–14786; b) J. Wade, J. R. Brandt, D. Reger, F. Zinna, K. Y. Amsharov, N. Jux, D. L. Andrews, M. J. Fuchter, *Angew. Chem. Int. Ed.* **2021**, *60*, 222–227; c) F. Zhang, F. Rauch, A. Swain, T. B. Marder, P. Ravat, *Angew. Chem. Int. Ed.* **2023**, 62, e202218965.

[5] L. Arrico, L. Di Bari, F. Zinna, *Chem. Eur. J.* **2021**, *27*, 2920–2934.

[6] a) H. Tanaka, M. Ikenosako, Y. Kato, M. Fujiki, Y. Inoue, T. Mori, *Commun. Chem.* **2018**, *1*, 38; b) Y. Appiarius, S. Míguez-Lago, P. Puylaert, N. Wolf, S. Kumar, M. Molkenthin, D. Miguel, T. Neudecker, M. Juríček, A. G. Campaña, A. Staubitz, *Chem. Sci.* **2023**; c) Y. Liu, Z. Ma, Z. Wang, W. Jiang, *J. Am. Chem. Soc.* **2022**, *144*, 11397–11404.

[7] a) Y.-Y. Ju, L. Chai, K. Li, J.-F. Xing, X.-H. Ma, Z.-L. Qiu, X.-J. Zhao, J. Zhu, Y.-Z. Tan, *J. Am. Chem. Soc.* **2023**, *145*, 2815–2821; b) B. Liu, M. Böckmann, W. Jiang, N. L. Doltsinis, Z. Wang, *J. Am. Chem. Soc.* **2020**, *142*, 7092–7099; c) C. M. Cruz, I. R. Márquez, S. Castro-Fernández, J. M. Cuerva, E. Maçôas, A. G. Campaña, *Angew. Chem. Int. Ed.* **2019**, *58*, 8068–8072.

[8] a) T. Fujikawa, Y. Segawa, K. Itami, *J. Am. Chem. Soc.* **2015**, *137*, 7763–7768; b) J. Tan, X. Xu, J. Liu, S. Vasylevskyi, Z. Lin, R. Kabe, Y. Zou, K. Müllen, A. Narita, Y. Hu, *Angew. Chem. Int. Ed.* **2023**, *62*, e202218494; c) Y. Wang, Z. Yin, Y. Zhu, J. Gu, Y. Li, J. Wang, *Angew. Chem. Int. Ed.* **2019**, *58*, 587–591.

[9] a) J.-K. Li, X.-Y. Chen, W.-L. Zhao, Y.-L. Guo, Y. Zhang, X.-C. Wang, A. C.-H. Sue, X.-Y. Cao, M. Li, C.-F. Chen, X.-Y. Wang, *Angew. Chem. Int. Ed.* **2023**, *62*, e202215367; b) P. Izquierdo-García, J. M. Fernández-García, S. Medina Rivero, M. Šámal, J. Rybáček, L. Bednárová, S. Ramírez-Barroso, F. J. Ramírez, R. Rodríguez, J. Perles, D. García-Fresnadillo, J. Crassous, J. Casado, I. G. Stará, N. Martín, *J. Am. Chem. Soc.* **2023**, *145*, 11599–11610; c) X. Tian, K. Shoyama, B. Mahlmeister, F. Brust, M. Stolte, F. Würthner, *J. Am. Chem. Soc.* **2023**, *145*, 9886–9894; d) J. Hong, X. Xiao, H. Liu, E. Dmitrieva, A. A. Popov, Z. Yu, M.-D. Li, T. Ohto, J. Liu, A. Narita, P. Liu, H. Tada, X.-Y. Cao, X.-Y. Wang, Y. Zou, K. Müllen, Y. Hu, *Chem. Eur. J.* **2022**, *28*, 202202243; e) S. Míguez-Lago, I. F. A. Mariz, M. A. Medel, J. M. Cuerva, E. Maçôas, C. M. Cruz, A. G. Campaña, *Chem. Sci.* **2022**, *13*, 10267–10272.

[10] W. Niu, Y. Fu, Z.-L. Qiu, C. J. Schürmann, S. Obermann, F. Liu, A. A. Popov, H. Komber, J. Ma, X. Feng, *J. Am. Chem. Soc.* **2023**, *145*, 26824–26832.

[11] a) Y.-J. Shen, N.-T. Yao, L.-N. Diao, Y. Yang, X.-L. Chen, H.-Y. Gong, *Angew. Chem. Int. Ed.* **2023**, *62*, e202300840; b) Y. Chen, C. Lin, Z. Luo, Z. Yin, H. Shi, Y. Zhu, J. Wang, *Angew. Chem. Int. Ed.* **2021**, *60*, 7796–7801.

[12] Deposition Numbers 2308316 (***m*ED7H**) and 2308317 (***p*ED7H**) contain the supplementary crystallographic data for this paper. These data are provided free of charge by the joint Cambridge Crystallographic Data Centre and Fachinformationszentrum Karlsruhe Access Structures service.

[13] a) T. Lu, F. Chen, *J. Comput. Chem.* **2012**, *33*, 580–592; b) T. Lu, Q. Chen, *J. Comput. Chem.* **2022**, *43*, 539–555.

[14] a) Y. Hu, X.-Y. Wang, P.-X. Peng, X.-C. Wang, X.-Y. Cao, X. Feng, K. Müllen, A. Narita, *Angew. Chem. Int. Ed.* **2017**, *56*, 3374–3378; b) X.-Y. Wang, X.-C. Wang, A. Narita, M. Wagner, X.-Y. Cao, X. Feng, K. Müllen, *J. Am. Chem. Soc.* **2016**, *138*, 12783–12786; c) Y. Hu, G. M. Paternò, X.-Y. Wang, X.-C. Wang, M. Guizzardi, Q. Chen, D. Schollmeyer, X.-Y. Cao, G. Cerullo, F. Scotognella, K. Müllen, A. Narita, *J. Am. Chem. Soc.* **2019**, *141*, 12797–12803.

[15] J. M. Fernández-García, P. Izquierdo-García, M. Buendía, S. Filippone, N. Martín, *Chem. Commun.* **2022**, *58*, 2634–2645.

Manuscript received: December 22, 2023
Accepted manuscript online: February 19, 2024
Version of record online: ■■, ■■

Research Articles

Chiral Nanographenes

W. Niu,* Y. Fu, Q. Deng, Z.-L. Qiu, F. Liu, A. A. Popov, H. Komber, J. Ma,* X. Feng **e202319874**

Enhancing Chiroptical Responses in Helical Nanographenes via Geometric Engineering of Double [7]Helicenes

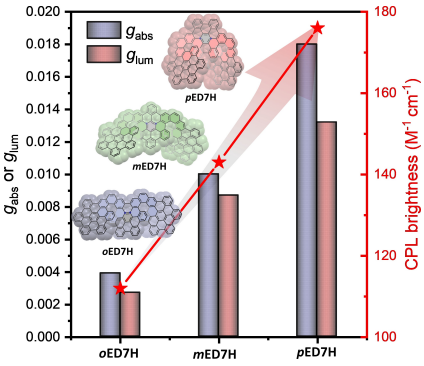

π-Extended helical nanographenes (**ED7Hs**) have been synthesized where the two embedded [7]helicene units are fused at the *ortho*-, *meta*- or *para*-position of the middle benzene ring, respectively. The obtained **ED7Hs** display exceptional fivefold amplification in chiroptical responses with enhanced circularly polarized luminescence (CPL) brightness up to 176 M^{-1} cm^{-1}.